



HAL
open science

Monitoring soil water content and its salinity with high-precision and low-cost in-situ sensors

Xavier Chavanne, Jean-Pierre Frangi

► **To cite this version:**

Xavier Chavanne, Jean-Pierre Frangi. Monitoring soil water content and its salinity with high-precision and low-cost in-situ sensors. *European Journal of Environmental and Civil Engineering*, 2023, 27 (1), pp.457-478. 10.1080/19648189.2022.2051076 . hal-04055985

HAL Id: hal-04055985

<https://cnrs.hal.science/hal-04055985v1>

Submitted on 3 Apr 2023

HAL is a multi-disciplinary open access archive for the deposit and dissemination of scientific research documents, whether they are published or not. The documents may come from teaching and research institutions in France or abroad, or from public or private research centers.

L'archive ouverte pluridisciplinaire **HAL**, est destinée au dépôt et à la diffusion de documents scientifiques de niveau recherche, publiés ou non, émanant des établissements d'enseignement et de recherche français ou étrangers, des laboratoires publics ou privés.

Monitoring soil water content and its salinity with high-precision and low-cost in-situ sensors

Xavier Chavanne^a and Jean-Pierre Frangi^a

^aUniversité de Paris, Institut de physique du globe de Paris, UMR 7154 CNRS, F-75205 Paris cedex 13, France

ARTICLE HISTORY

Compiled April 3, 2023

CONTACT X. Chavanne. Orcid 0000-0002-2199-4943 Email: xavier.chavanne@u-paris.fr

ABSTRACT

The article presents **an** in-situ sensor to monitor soil moisture and water salinity **by measuring** soil permittivity and conductivity at a frequency 24 MHz via an admittance approach. It addresses difficulties encountered in other permittivity-based sensors. A self-balanced bridge provides on one measurement a digital output linear to capacitance and conductance of electrodes in soil with low offset, high phase resolution, and taking into account all parasitic impedances. Circuit design and procedures to achieve it are described, using electric circuit theory and component specifications. Probe geometry, two parallel cylinders, permits insertion in soil from surface, low disturbances and a high sample volume around electrodes. It provides an analytical relation to convert admittance to soil permittivity.

Calibration of a sensor with air, alcohols and water fixes its sensitivity and residual phase and inductance for an uncertainty lower than 2% over a range up to 80 and 200 mS·m⁻¹. Identical sensors can use same parameters after adjusting in one simple operation bridge phases. Thermal drift and its consequences on soil variable measurement are investigated and physical origins identified. It permits to reduce the phase drift within $\pm 150\text{ppm}\cdot\text{C}^{-1}$ rad to keep accuracy.

KEYWORDS

in-situ sensor; soil water content; salinity; complex permittivity; self-balanced admittance bridge; electronics drift

1. Introduction

The article presents an in-situ sensor able to monitor key variables of a soil such as its water content (Θ_V) and water salinity (σ_{ion}) at a depth or along a profile. Sensor relies on the measurement of permittivity ϵ_r of a soil and its conductivity σ , which vary with Θ_V and σ_{ion} . The device produces a rapid response linear to soil quantities ϵ_r and σ with potential deviations intrinsically or automatically compensated. These features and other characteristics facilitate sensor duplication and use at reduced cost, and its integration into networks for field autonomous and continuous operations. **Sensors integrate circuits to acquire and process data, and to manage the operations. It uses recent technology of communication to send data once measured in a web-accessed data base where data are retrieved.** Networks of in-situ sensors to determine fields of soil variables over large surfaces offer a good alternative to large-volume averaging and **more** indirect instruments, such as remote sensing from space or air-born radiometers based on surface emissivity [Schmugge, Kustas, Ritchie, Jackson, and Rango (2002)] and counters of neutrons produced from cosmic rays and backscattered by H atom present in soil [Zreda et al. (2012)].

We limit the scope of present article to the instrument, and do not deal with the control and communication part of the sensor to obtain networks of autonomous and wireless sensors. This is the object of an article recently submitted.

Soil - the about one-meter-thick piece of land in contact with atmosphere and substrate of plant roots - is able to store some water within its pores and to restore it at time scales from few hours to years, depending on its structure. This capability is crucial in soil interaction with other environment components through the water, energy and material cycles, like atmosphere, subsoil, plants... and to control natural phenomena such as landslide and drought from short-term forcing (a strong rain or a dry period), and local climate change in longer terms. Monitoring Θ_V is not only necessary in meteorological and climate models, but also in agriculture for effective irrigation, in industrial processes to control material quality (like for concrete) and

their aging. Water salinity in soil is important to measure as well to infer nutrient quantity for plants or to control potential contamination from leaching [Rhoades and Chanduvi (1999)].

Whereas air is a gas made homogeneous thanks to convection, soil is an heterogeneous and multi-phase medium where diffusive mechanisms dominate for transport. As a consequence, air relative humidity is easy to measure, not soil moisture.

The standard method—soil sample weighting and drying in oven—provides directly the mass of water content, but is too destructive and human-time consuming for continuous automated monitoring [Reynolds (1970)].

One of the most promising methods to meet these objectives is based on soil dielectric permittivity. Permittivity measures the strength of medium electric dipoles to respond to the electric field induced by the sensor. The normalized or relative quantity, ε_r (using the vacuum permittivity $\varepsilon_0 = 8,854 \text{ pF.m}^{-1}$ for reference), is $\varepsilon_r = 80$ for water at 20°C, due to its strong molecular dipoles, whereas it varies from $\varepsilon_r = 2$ to 5 for a dry soil, and is $\varepsilon_r = 1$ for air (confounded with that of vacuum). Literature abounds on relations of conversion of ε_r into Θ_V , from extended Archie’s laws [Revil (2013)] to Topp’s empirical correlation [Topp, Davis, and Annan (1980)]. Moreover, instruments relying on this principle can provide output easily digitized, and their operations be automated.

Permittivity should not be confused with soil conductivity σ , which results in part from water free charges or ions, and not its molecular dipoles. From a theoretical point of view the two quantities ε_r and σ are intricately linked in the equations governing electromagnetic fields in a medium. For this reason ε_r and σ are grouped together within the complex expression ε_r of the relative permittivity (with $\mathbf{j}^2 = -1$):

$$\varepsilon_r = \varepsilon_r - \mathbf{j} \frac{\sigma}{\varepsilon_0 2\pi f}, \quad (1)$$

where f is the frequency of the electric field applied.

Resolution of the equations in case of porous media like soils and rocks, owing to many simplifications, constitutes the bulk of the literature devoted to the ε_r - Θ_V conversion (see for instance [Chelidze, Gueguen, and Ruffet (1999); Hilhorst (1998); Revil (2013)]). Formally, the expression 1 is valid over a frequency range from mHz to 1 GHz, provided each part in ε_r includes terms associated to mechanisms in the medium other than those resulting from water dipoles or its ions. Their importance depends on the frequency range of f . For instance below $f = 10 \text{ MHz}$ ions close to grain surface act as dipoles of which permittivity exceeds that of water molecules [Campbell (1990); Chelidze and Gueguen (1999); Descarpentries (1966); Eller and Denoth (1996); Sen and Chew (1983); Kessouri (2012)]. Due to thermal diffusivity each type of dipoles presents a relaxation or phase delay to follow the direction of an electric field, when f rises past the characteristic frequency f_{rlx} of the dipoles [Debye (1929)]. The effect reduces the contribution of the dipoles to ε_r , down to zero as $f \gg f_{rlx}$. It increases σ around f_{rlx} , independently of ion transport.

Already many sensors have been developed along the permittivity principle, and commercialized. Actually, each manufacturer specializes in a particular measurement technique to determine soil water content. The same technique is used to the family of products proposed by the manufacturer. They only differ by electrode geometry or by adding new features such as converting instrument analog output to a digital one. Although their range is wide, we can classify techniques according to how they exploit

electromagnetic fields to sense ε_r (see also [Chavanne and Frangi (2017)]):

- Those using the phase velocity or travel time of an electromagnetic wave propagating along a guide in a soil. The velocity varies with the real part of the root square of ε_r (eq. 1), approximated to ε_r at low conductivity.
- Others operating with the amplitude of sensor electromagnetic fields to determine the capacitance (or admittance if they are able to measure simultaneously the conductance part in parallel) of electrodes embedded in a soil. Their output can be potentially linear to ε_r .

Commonly used sensors of the propagation group are the Time Domain Reflectometry Systems (TDRs). They are composed of a step-pulse generator and a waveform analyzer connected to probes in soil (e.g. the module TDR100 with probes CS659, commercialized by Campbell Scientific Inc., Logan, UT, USA [“TDR100 user guide” (2015)]). Because their output, pulse-travel time along the guide, is readily related to soil permittivity, TDRs gained a sort of standard status as in-situ soil moisture sensors. Guide consists in simple parallel rods inserted in soil, of which the open ends induce a partial reflection (a transmission version with the guide in the form of loop also exists). Topp established in 1980 his correlations between ε_r and Θ_V thanks to these sensors [Topp et al. (1980)]. However, high-speed electronics to generate the step excitation, record the return wave and determine a time of travel from the waveform make them costly and energy consuming, which prevent TDRs from continuous monitoring in an autonomous mode. Even the last product of Campbell Scientific, TDR soilvue [“SoilVUETM10 Manual” (2019)], which is more compact and able to measure various soil variables at different depths, remain expensive and difficult to operate autonomously (its price for 6 channels amounts to 1700 \$ w/o VAT, not including the external datalogger required to store its digital output and assure their transfer).

A compact and low-cost version of TDRs, called reflectometer, consists in an electronic ring oscillator which triggers an impulse once it receives the return wave [Qu, Bogena, Huisman, and Vereecken (2013)]. It generates thus a cyclic output of which period is related to the wave travel time. Campbell Scientific proposes some of them, like CS616 and more recently CS650, the digital version [“CS650 and CS655 Water Content Reflectometers Manual” (2016)]. However, the output is not as directly related to travel time as for TDRs, such as Campbell Scientific did not retain the technique for its last product.

Sensors belonging to the capacitance family are cheaper than TDRs due to the use of lower electronic speed (signal-rise time higher than few ns, versus less than 10 ps in the case of TDRs). They operate at a frequency f close to or lower than 100 MHz. At this frequency electromagnetic wavelength in air is 3 m - but only 60 cm at $\varepsilon_r = 25$ -, higher than a typical electrode dimension of 10 cm. Sensor circuit and its output can be modeled and interpreted thanks to the electric circuit theory [Hilhorst (1998); Kelleners et al. (2004)], which assumes negligible propagation effect. Sensor electrodes embedded in a soil form a capacitor which is represented by an admittance composed of electrode capacitance C and conductance G in parallel, $Y = G + \mathbf{j} C 2\pi f$. Hence Y is readily related to the apparent permittivity of the medium ε_r in eq. (1):

$$\varepsilon_r = \frac{C}{\varepsilon_0 g} - \mathbf{j} \frac{G}{\varepsilon_0 g 2\pi f} = -\mathbf{j} \frac{Y}{\varepsilon_0 g 2\pi f} . \quad (2)$$

where g is a factor with unit of length depending only on electrode design and dimensions. In the case of the bi-cylindrical geometry adopted for our sensors it varies from

0.1 to 0.15 m (see in section 2.3).

Range of techniques to determine Y or, in most cases, only C are wide. They are intended to reduce costs but at the expense of accuracy. EnviroSCAN and recent TriSCAN probes marketed by Sentek Pty Ltd., Stepney, Australia give the frequency of an electronic oscillator consisting of an inductor and a capacitor in parallel [Kelleners et al. (2004)]. The capacitor is partly made of electrodes in soil. Decagon Devices Inc., Pullman, WA, USA (now METER group) commercializes sensors which use the root mean square of partial-charging cycles of the same capacitor (from ECH₂O to GS3, including EC5, 10HS, 5TE...) [H. Bogena, Huisman, Oberdörster, and Vereecken (2007)]. An hybrid method uses the propagation and reflection of a sinus wave in a coaxial line ended by the electrodes [Campbell (1990); Gaskin and Miller (1996)]. From the complex coefficient of reflexion at the end of the coaxial line is determined line terminal impedance. It corresponds to the impedance of electrodes considered as an open ended transmission line of which permittivity is that of soil. Sensors of Stevens System (Portland, OR, USA), such as HydraProbe, as well as those of Delta_T Devices Ltd. (Cambridge, UK), like PR2 and Theta Probe, are based on this technique, each operating at one frequency (50 and 100 MHz, respectively). In the case of Delta_T sensors, due to multiple reflexions at coaxial and probe ends (propagation effect at $f = 100$ MHz), an empirical approach is necessary and limits instrument output to permittivity [Gaskin and Miller (1996)]. HydraProbe provides both ε_r and σ , but no information on the precise procedure is available.

Attempts have been made to determine more directly the admittance Y in eq. 2, based on Ohm's law. The difficulty lies in the phase detection of Y . In the 1990s, Hilhorst designed an application-specific integrated circuit to determine Y at $f = 20$ MHz [Hilhorst (1998)]. The circuit contained in particular actuated switches, phase shifters and synchronous detectors to separate the two components of Y . Because of the poor accuracy of component gains - $\pm 20\%$ -, of phase errors (up to 15 degrees) and high sensitivity to temperature, measurement of on-board references must be carried out alongside each electrode measurement to offset errors [Hilhorst (1998)]. From this work a sensor was developed and commercialized by Delta-T Devices Ltd, WET Sensor, which outputs both ε_r and σ . To avoid the phase-resolution difficulty, Rêgo et al. proposed to measure the amplitude of Y at two distinct frequencies, 500 kHz and 8 MHz [Rêgo Segundo, Martins, Monteiro, de Oliveira, and Freitas (2015); Rêgo Segundo, Silva Pinto, Almeida Santos, and de Barros Monteiro (2019)]. C and G are determined by calculating the expression of Y amplitude at both frequencies. However, because of circuit parasitic impedances not accounted for, separation of the two parts of Y is still complex, requiring multi-parameter correlations. Moreover, choice of frequencies may pose a problem due to dipole relaxations in this range.

In summary most of techniques based on ε_r to determine soil moisture are simple enough to reduce their cost, but determination of soil permittivity is often too indirect. Manufacturers have to resort to empirical conversions to obtain ε_r from instrument output, if they provide it at all. Indeed, they prefer to give a correlation between output and soil water content from calibration with soil samples. These correlations are specific to the instrument and to type of soil, as they include effects from both without discrimination. All literature on soil permittivity becomes useless. The oversimplification of these techniques makes often the physical modeling of their operations difficult and thus prevents some in-depth understanding. Kelleners et al. showed the interest of this type of study in the case of Enviroscan: a simple electric circuit of which components are identified to sensor parts (inductor, access tube...) explains the low dependence of LC-oscillator frequency to medium permittivity above 30, as well

as its strong dependence on conductance [Kelleners et al. (2004)]. Above a medium conductivity of $100 \text{ mS}\cdot\text{m}^{-1}$ sensor output is dominated by σ not ε_r .

To put in evidence sensor artifacts independently of soil related effects, a sensor must be tested with actual standards of complex permittivity like liquids of known permittivity and conductivity σ , as stressed by Jones et al. [Jones, Blonquist, Robinson, Rasmussen, and Or (2005)]. They also assure a better contact with electrodes than a soil. The authors provided guidelines to characterize a sensor and its output: sensitivity to ε_r , influences of instrument temperature and of medium conductivity, medium sample volume... They evaluated seven commercial sensors as an illustration [Blonquist, Jones, and Robinson (2005)]. Three of them were based on waveform analysis to retrieve a time travel, like TDR100. Conversion to ε_r is based on the same physical dependence of electromagnetic speed to ε_r . For accuracy actual value of the guide length is determined with liquid calibration. Each of other sensors - CS616, HydraProbe, Theta Probe and ECH₂O - necessitates an empirical relation deduced from liquid calibration or given by the manufacturer when available. It presents a non linear relation, with low sensitivity beyond ε_r 20 to 30 except for the reflectometer CS616. As far as sensitivity to conductivity is concerned, output of time travel sensors presents an increasing dependence, with an error of about $\delta\varepsilon_r = \pm 1$ at $\sigma = 100 \text{ mS}\cdot\text{m}^{-1}$ and $\delta\varepsilon_r = \pm 3$ at $\sigma = 200 \text{ mS}\cdot\text{m}^{-1}$. Except HydraProbe of behavior similar to TDRs, other sensors show bigger influence (error of $\delta\varepsilon_r \approx \pm 10$ at $\varepsilon_r = 40$ and $\sigma = 100 \text{ mS}\cdot\text{m}^{-1}$, increasing beyond). Sensor ECH₂O is even more impacted (negative value at $\varepsilon_r = 40$ and $\sigma = 100 \text{ mS}\cdot\text{m}^{-1}$). Study of temperature influence requires standards which do not vary with temperature or are corrected from the variation, especially for sensors of which guide or electrodes are directly attached to electronics. The layout makes difficult to control electronics temperature independently of electrode one. Authors of the study have to determine variations of liquid permittivity with temperature before sensor characterization [Jones et al. (2005)], which adds some uncertainty. At the end of the day they report for time travel sensors an absolute drift of $\delta\varepsilon_r \approx +0.1$ to $0.15 \text{ }^\circ\text{C}^{-1}$ between 5 to 40°C and around $\varepsilon_r = 40$, or a relative one of $+3\,500 \text{ ppm}\cdot^\circ\text{C}^{-1}$ (ppm: part per million). Sensors CS616, HydraProbe and ECH₂O present similar drifts, being lower for Thetaprobe. Seyfried et al., using air of which ε_r remains constant with temperature, reported for the previous version of CS616, CS615, an absolute drift for sensor output of $-0.0005 \text{ ms}\cdot^\circ\text{C}^{-1}$ around an average of 0.745 ms , or a relative drift of $-700 \text{ ppm}\cdot^\circ\text{C}^{-1}$. Sign and amplitude is not the same as for CS616. Is this because working with a too low permittivity? using a different sensor although with the same technique? or is it resulting from natural dispersion of specifications of sensor electronic parts? An empirical study with limited number of sensors can not answer the questions.

Models EC5 and 5TE, proposed after ECH₂O by Decagon (5TE provides a multi-variable digital output), were studied thoroughly by Rosenbaum et al using the same methodology as for Jones et al [Rosenbaum, Huisman, Vrba, Vereecken, and Bogena (2011)]. They intended to establish empirical algorithms to correct for influences of instrument temperature and medium conductivity, taking into account cross-correlation with permittivity (up to ten coefficients for each influence). They provide as well an empirical relation to convert sensor output into ε_r . Ten sensors for each product were tested in an attempt to account for sensor variability [Rosenbaum, Huisman, Weuthen, Vereecken, and Bogena (2010)]. Mixtures of 2-isopropoxyethanol and water were used for the work. Their permittivity and its dependence with temperature and frequency were determined during the work. Typically, relative drift of liquid ε_r due to temperature is about $-6\,000 \text{ ppm}\cdot^\circ\text{C}^{-1}$. Instrument relative drift varies with permittivity

from about $-3\,000\text{ ppm}\cdot\text{C}^{-1}$ at $\varepsilon_r = 20$ to $-5\,000\text{ ppm}\cdot\text{C}^{-1}$ at $\varepsilon_r = 40$. Sensitivity to conductivity is lower than for ECH₂O sensor but still important, depending on ε_r : at $\varepsilon_r = 40$ absolute error varies from $\delta\varepsilon_r = -9$ at $\sigma = 100\text{ mS}\cdot\text{m}^{-1}$ to $\delta\varepsilon_r = -4$ at $250\text{ mS}\cdot\text{m}^{-1}$ while at $\varepsilon_r = 26$ error $\delta\varepsilon_r$ varies from -5 at $50\text{ mS}\cdot\text{m}^{-1}$ to $+6$ at $250\text{ mS}\cdot\text{m}^{-1}$. In the case of Decagon recent product GS3, it is observed in water - $\varepsilon_r = 80$ - a decrease of $\delta\varepsilon_r = -21$ at $\sigma = 180\text{ mS}\cdot\text{m}^{-1}$ (Figure 6 in [Chavanne and Frangi (2017)]).

Along with the digital conversion of measurements, manufacturers have added for its own interest conductivity measurement to their recent products (as well as soil temperature at electrode level): TDR soilvue and reflectometers CS650 of Campbell Scientific, TriSCAN probe for Sentek Pty, 5TE and GS3 for Decagon/Meter..., while keeping the same technique to determine soil water content. Both techniques are thus independent, for instance they do not operate at the same frequency (except for WET Sensor. Information about hydraprobe is insufficient to decide on it). Exists the risk of measuring a conductivity different from the conductivity at f used in eq. (1), due to the contribution from dipole relaxations depending on f . Sensors of Campbell Scientific use the amplitude attenuation of trains of $20\text{-}\mu\text{s}$ -wide pulses at 10 kHz frequency [Bechtold, Huisman, Weihermüller, and Vereecken (2010)]. Moreover, it does not seem that this capability is used to correct conductivity influence on permittivity measurement. No real difference on output sensitivity between EC5 and 5TE or GS3 of Decagon. Only Campbell Scientific reports for CS650 the use of an algorithm to correct σ dependence.

The development of our own technique - self-balanced bridge - is intended to address the difficulties encountered in previous sensors. It uses a capacitance approach, actually an admittance one by measuring simultaneously the two quantities C and G in eq. 2. Hence a linear relation is obtained from sensor output to soil apparent complex permittivity at a frequency f (currently 24 MHz), as expressed in eq. 1.

Section 2 exposes instrument characteristics and procedures to obtain an output linear to ε_r and σ . Electric circuit theory is used to model the instrument analytically and determine any deviation from linearity, interferences between measured C and G , and other influences on its output. The work links these errors to different parts of the sensor and their known characteristics. The section details modifications on circuit and procedures to offset or reduce the errors, and gives physical relations to account for residues. Physical relations, along with component specifications, allow to assess importance of these errors over the whole range of sensor operation, before any calibration, which is not possible with empirical relations. Choices for sensor design - electronics at surface and bi-cylindrical geometry for parts in soil - are justified to reach simplicity, low disturbance, ease of installation and a large sample volume. Drawbacks - e.g. long lead - are dealt with.

The section 3 presents results from calibration of a sensor with pure liquids and some saline solutions. Electronics drift from thermal variations are studied in detail to identify its physical origin and assess its impact on the final result, water content and salinity during field trials. On-board reference admittance with low drift is used for this work. Means to reduce the drift are indicated.

Design of the instrument has to incorporate constraints of costs and energy consumption by limiting the number of parts, using standard and efficient ones, and by simplifying procedures specific to each sensor. The compromise with measurement quality is detailed. The work is in a research and development phase with successive generations of two or three prototypes.

2. Materials and Methods



Figure 1. One-channel sensor of last generation during a field trial. Box containing electronics, and aerial part of lead towards electrodes in the soil.

The instrument is made of a sensing part - pair(s) of cylindrical stainless steel electrodes in the soil -, the lead to connect the electrodes to measuring electronics, and the measuring circuit itself inside a separate box at the soil surface (Fig. 1). The housing contains as well units of analog-to-digital conversion, processing and communication assembled in a separate circuit, presently. Battery is enclosed within. Electronics is not compact enough to be inserted in cylinders. The choice is also motivated to have a **better radio transmission than being buried** and an ease of intervention (for a change of battery). Box dimensions are 14 cm by 14 cm in surface and 6 cm in height, in the case of the last generation sensor (a more compact housing will be used for the next generation). It is fitted with 3 cm high legs at its corners to isolate it from soil surface. The box is **laterally 10 cm apart from the point where electrodes are inserted in order** to limit perturbations on rain-flow patterns above ground.

Sensor design avoids to dig a trench and permits a rapid installation in soil. Two parallel holes are first bored with a large guide from soil surface. The pair of cylinders containing lead and electrodes are inserted, maintained parallel with a spacer, which is removed after installation. A permanent spacer between electrodes, or above, will modify flow of water around them, and therefore will make measurement of moisture not representative of it in soil beyond electrode sampling volume. **There may be a risk of a change of electrode spacing due to soil movements. However, we do not observe this as the pair of cylinders in soil still fits the spacer after several months of experiment.**

Two types of sensors are developed according to their number of pair of electrodes. Multi-channel sensors measure soil variables at different depths thanks to stacked electrodes on same cylinders [Chavanne and Frangi (2014)]. They share the same measuring circuit. Controlled relays connect successively the different pair of electrodes to the circuit. A one-channel sensor has a unique pair of electrodes to determine soil variables at one depth. The electrode geometry is identical for both sensors, with size smaller in the case of one-channel sensor.

Following subsections detail the sensor chain of conversion from raw data - circuit output - to admittance of electrodes in soil, to soil permittivity according to three stages:

- **Determination of admittance at the input of measuring circuit taking into account its sensitivity, offset and phase errors.**

- Accounting for parasitic impedances of lead.
- Conversion of electrode admittance to soil complex permittivity.

We also indicate the relations presently used to convert permittivity into soil moisture and its water salinity for field measurements.

2.1. Self-Balanced Wheatstone Bridge

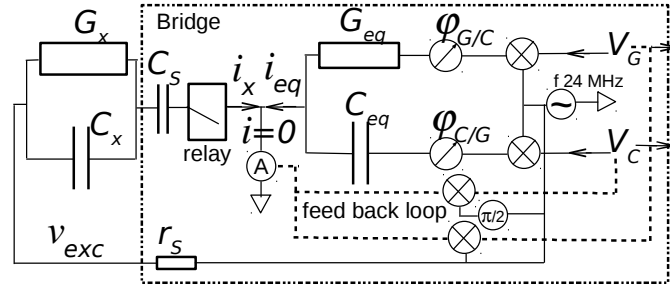


Figure 2. Schematic diagram of the self-balanced Wheatstone bridge to measure conductance G_x and capacitance C_x at frequency f . Bridge excitation at f , v_{exc} , is provided by a quartz-tuned analog oscillator. A feedback loop assures a fast equilibrium and provides direct voltages V_G and V_C proportional to G_x and C_x with respective coefficients G_{eq} and C_{eq} . A controlled relay and phase shifters $\varphi_{G/C}$ and $\varphi_{C/G}$ permit to correct deviations from perfect linearity and phase resolution. **When connected to electrodes through a lead** a resistor r_S and a capacitor C_S in series ensure protection and compensation of wire inductance (see subsection 2.2).

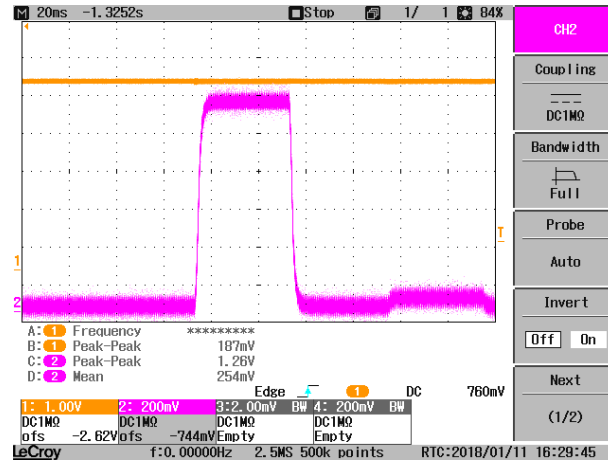


Figure 3. Screen shot of an oscilloscope in recording mode. Bridge analog output of the capacitive branch V_C - see Fig. 2 - is recorded when a sensor channel with high capacitance is connected. Bridge reaches its new equilibrium in less than 10 ms (time division of 20 ms. Noise in amplitude due to low resolution of oscilloscope).

The core technology of the measuring circuit is a self-balanced Wheatstone bridge, of which a simplified diagram is shown Fig. 2. The entire circuitry is analog. It determines at a frequency f the admittance $Y_x = G_x + jC_x 2\pi f$ at its input through two direct voltages, V_G and V_C , each proportional to one admittance part, conductance G_x or capacitance C_x . **The situation corresponds to an on-board admittance Y_x with resistance $r_S = 0 \Omega$ and infinity capacitance C_S in series.** Bridge contains two branches, similar on their structure, each dedicated to one part of Y_x . An excitation

voltage v_{exc} , from a quartz-tuned oscillator, is applied between admittance ends. The resulting current i_x is balanced owing to a feedback loop made of a current/voltage converter, and a de-modulator and an integrator in each branch. Feedback input is the unbalanced signal at f . Integrator output are the feedback DC voltage V_c and V_g which build up until the bridge is balanced and signal sent to demodulators becomes zero. The loop thus provides V_G and V_C proportional to each part of the current to be balanced, and, as a result, to G_x and C_x . Voltages are fed to modulators to construct the alternating current i_{eq} which offsets i_x . Voltages are limited by component supply and linearity conditions to a range from -3.5 to 3.5 V. They are digitized by an Analog-to-Digital Converter (A/DC) in the digital circuit. Data reported in the whole article, except in Fig. 3, correspond to the digitalized output. In the case of last generation sensors voltages are digitized by a bipolar 24-bit A/DC (MCP3903-I/SS of Microchip Technology Inc.), after a voltage division by 7 to accommodate ADC full scale of 1 V. Considering 22 as the effective number of bits the theoretical resolution would be few μV . Actually, due to bridge noise, we observe a resolution of ± 0.2 mV from repeatability of measurements at same bridge input. For one measurement the A/D converter performs a sampling to reduce the noise (typ. 50 samples).

Bridge equilibrium is reached in less than 10 ms (screen shot of an analog output in Fig. 3 when a new admittance is connected), which permits to lower its time of activation. This feature and direct voltages as an output make the bridge suitable for continuous measurement in real time in an autonomous device.

Ideally bridge output should verify:

$$\begin{cases} G_x = G_{eq} V_G, \\ C_x 2\pi f = C_{eq} 2\pi f V_C, \end{cases} \quad (3)$$

Parameters G_{eq} and C_{eq} are bridge sensitivity parameters. Their values are fixed by amplifier gains, a voltage divisor and either a resistance or a capacitance according to the branch. **These components - mainly resistors - are chosen to present a low dispersion from their nominal value, such as 0.1% for resistors and 1% for capacitors. As a result, bridges of a series of same sensors, i.e. with identical components, will present same sensitivity within specification uncertainty of the critical components. A reference admittance on bridge circuit - see further down - permits as well to control the values of G_{eq} and C_{eq} . Uncertainty on G_{eq} and C_{eq} is assessed as 1%.**

Sensitivity parameters are usually varied from $G_{eq} = 5$ to $10 \text{ mS}\cdot\text{V}^{-1}$, and from $C_{eq} = 30$ to $50 \text{ pF}\cdot\text{V}^{-1}$. Combining eq. 3 with eq. 2 with a value of 0.14 m for g (assuming also parasitic impedances seen in subsection 2.2 negligible), and taking into account V_G and V_C range, the capacitive branch covers a ϵ_r range corresponding to values from air to water. The conductive one measures up to around $150 \text{ mS}\cdot\text{m}^{-1}$ (or $1500 \text{ }\mu\text{S}\cdot\text{cm}^{-1}$). It is possible to raise G_{eq} to extend the range of soil conductivity, at the cost of resolution.

Actually, the linear relationship of eq. 3 corresponds to ideal operations of the bridge in which no offset and phase errors exist. We examine now how to compensate them automatically or by a simple operation.

Correction of offsets A first departure from eq. 3 results from offsets of active components, which gives an output in absence of admittance Y_x . Correction is achieved owing to a processor-controlled relay. It disconnects the bridge from electrodes in order

to measure open circuit voltages V_{G0} and V_{C0} , in addition of V_G and V_C . Eq 3 is computed with their difference, $\Delta V_G = V_G - V_{G0}$ and $\Delta V_C = V_C - V_{C0}$. Residual offset would be about ± 0.3 mV.

As we will see in section 3.3 the operation permits equally to correct part of drifts with temperature of electronics. Furthermore, it avoids determination of V_{G0} and V_{C0} for each bridge of a series of same sensors, at the modest cost of a controlled relay. Indeed, as offsets differ due to specification dispersion for a same component, V_{G0} and V_{C0} vary from one bridge to another.

Correction of phase errors The main advantage of the bridge, of which digital electronics are still not capable at this frequency, is its phase resolution, i.e. its ability to discriminate, at the end of the chain of conversion, between soil water content and conductivity [Chavanne, Bruère, and Frangi (2018)]. The tangent of the phase θ of the complex permittivity (eq. 1) is:

$$\tan \theta = \frac{\varepsilon_r \varepsilon_0 2\pi f}{\sigma} = \frac{\varepsilon_r 1.33}{\sigma (\text{mS} \cdot \text{m}^{-1})} \simeq \frac{C_x 2\pi f}{G_x}. \quad (4)$$

Last equality assumes parasitic contributions of lead to be negligible (see next subsection). In this approximation θ is also the phase of the input admittance $Y_x = Y_{0x} e^{j\theta}$ or the inverse of the so-called loss angle.

Let's examine the condition on θ to retrieve accurately a variable when it is smaller than its complex conjugate. For a soil with a large apparent conductivity such as $\sigma = 200 \text{ mS} \cdot \text{m}^{-1}$ - or $2.00 \text{ mS} \cdot \text{cm}^{-1}$ - (according to Section 4 of [Hilhorst (1998)], the bulk conductivity for clayey soils can exceed $\sigma = 100 \text{ mS} \cdot \text{m}^{-1}$. In our trial in Alps σ remains below this value), to obtain the permittivity with a resolution of $\delta\varepsilon_r = \pm 0.1$ at 24 MHz, the system would need a phase resolution of $\delta\theta \simeq \pm 0.0007$ rad or 0.035° . It is inherently difficult, especially for a field sensor. The phase tangent itself for a typical permittivity $\varepsilon_r = 25$ is $\tan \theta = 0.16$. By comparison in the sandy soil of our plot conductivity can be of order of $\sigma = 10 \text{ mS} \cdot \text{m}^{-1}$ for a permittivity $\varepsilon_r = 8$, which gives $\tan \theta$ about 1. Both parts are of same importance. A resolution of $\delta\varepsilon_r = \pm 0.1$ requires a less stringent error of $\delta\theta \simeq \pm 0.015$ rad.

Limitation of the bridge on phase resolution results from phase **delays** of active components, up to -0.1 rad at 24 MHz. They induce interferences between the two branches of the bridge. Correction to obtain Y_x , at first order is:

$$\begin{cases} G_x \simeq G_{eq} \Delta V_G - \varphi_{C/G} C_{eq} 2\pi f \Delta V_C, \\ C_x 2\pi f \simeq C_{eq} 2\pi f \Delta V_C + \varphi_{G/C} G_{eq} \Delta V_G, \end{cases} \quad (5)$$

where $\varphi_{C/G}$ represents the overall phase error in the capacitive branch, while $\varphi_{G/C}$ is that in the conductive branch.

In order to keep this default negligible, a phase shifter with unity gain is added in each branch (represented by barred circles noted $\varphi_{C/G}$ or $\varphi_{G/C}$ in Fig. 2). Its transfer function T_{φ_Y} (symbol Y represents either C/G or G/C) is:

$$T_{\varphi_Y} = \frac{2}{1 - \mathbf{j}/(R_{\varphi_Y} C_{\varphi_Y} 2\pi f)} - 1 \simeq 1 + \frac{2\mathbf{j}}{R_{\varphi_Y} C_{\varphi_Y} 2\pi f}, \quad (6)$$

where R_{φ_Y} and C_{φ_Y} are values of the passive constituents of the shifter.

A $100\ \Omega$ potentiometer added in series with a $100\ \Omega$ resistor constitutes R_{φ_Y} . Potentiometer is adjusted to offset phase error φ_Y of each bridge branch. Capacitance C_{φ_Y} is usually $330\ \text{pF}$. As the quantity $R_{\varphi_Y} C_{\varphi_Y} 2\pi f$ is larger than 5, T_{φ_Y} is approximated in first order by the last expression in eq. 6. Its amplitude is close to one while its angle matches to $-\varphi_Y$ after adjustment. Its tangent is $\tan \varphi_Y \simeq 1/(R_{\varphi_Y} C_{\varphi_Y} \pi f)$.

Due again to specification dispersion phase errors differ from a bridge to another. As a consequence, shifters of each bridge must be adjusted against a reference. At the difference of the offset compensation with V_{G0} and V_{C0} , there is no automatic procedure to avoid a specific calibration. Nevertheless, the process is facilitated by the addition in bridge circuit of a channel with reference resistor R_{ref} and capacitor C_{ref} in parallel connected to the bridge through a controlled relay. The channel also permits to calibrate the values of bridges sensitivities G_{eq} and C_{eq} . To offset $\varphi_{G/C}$ in the G branch, capacitor is disconnected in the reference channel and the shifter is adjusted to reduce ΔV_C to zero at $\pm 0.3\ \text{mV}$ in eq. 5. Differentiating the equation gives a potential resolution for $\varphi_{G/C}$ with $R_{ref} = 220\ \Omega$ and $C_{eq} 2\pi f = 8.1\ \text{mS}\cdot\text{V}^{-1}$: $\delta\varphi_{G/C} \simeq R_{ref} C_{eq} 2\pi f \delta\Delta V_C = \pm 0.0005\ \text{rad}$.

The procedure assumes pure reference resistor and capacitor. In practice the resistor possesses a stray capacitance and the capacitor an equivalent series resistance ESR or a parallel loss. They are a surface-mount (SM) thin metal layer resistor and a SM ceramic multilayer capacitors of COG type, respectively, in a compromise between quality and cost (COG or NPO means temperature compensating with a drift lower than $\pm 30\ \text{ppm}\cdot\text{C}^{-1}$). To determine ESR we use a bridge and a high quality capacitor, ATC 100 B Series Porcelain Multilayer Capacitors, with ESR less than $0.02\ \text{Ohm}$ for $47\ \text{pF}$ below $100\ \text{MHz}$ i.e. a pure capacitor at $24\ \text{MHz}$ and bridge resolution. Bridge error $\varphi_{C/G}$ is thus offset. We then tested the standard COG capacitor with this bridge. It did not present a detectable phase, i.e. it also behaves like a pure capacitor at $24\ \text{MHz}$. As far as $\varphi_{G/C}$ is concerned an additional difficulty to stray capacitance is the existence of the inductance due to circuit traces, in series with the reference channel. By using a reference resistor of the same series or with same stray capacitance as of R_{ref} but with a higher resistance - $4K7\Omega$ -, in order to make negligible the inductance contribution in the output (see below in the case of lead), stray capacitance is determined as $0.2\ \text{pF}$. With the reference resistor of $220\ \Omega$ we can assess the parasitic bridge inductance (in the current design its value is $40\pm 3\ \text{nH}$), and even offset it by a capacitor like for the compensation of wire inductance presented below.

Because electronic devices present a drift with temperature change, shifters can introduce small perturbations during field measurement and deteriorate the phase resolution. The point is examined in the subsection 3.3.

At this stage bridge offsets and phase errors are corrected and its measurement sensitivity for capacitance and conductance is known within 1%. Bridges of a sensor series with identical component are interchangeable. They gave close output for a same admittance at bridge input.

We now look how to determine electrode admittance Y from the admittance Y_x .

2.2. Modeling Contributions of Lead and Electrodes to Measured Admittance

Fig. 4(a) breaks up the contributions to the admittance Y_x measured at bridge input. Admittance Y_{el} of electrodes at lead ends differs from Y , due specifically to medium

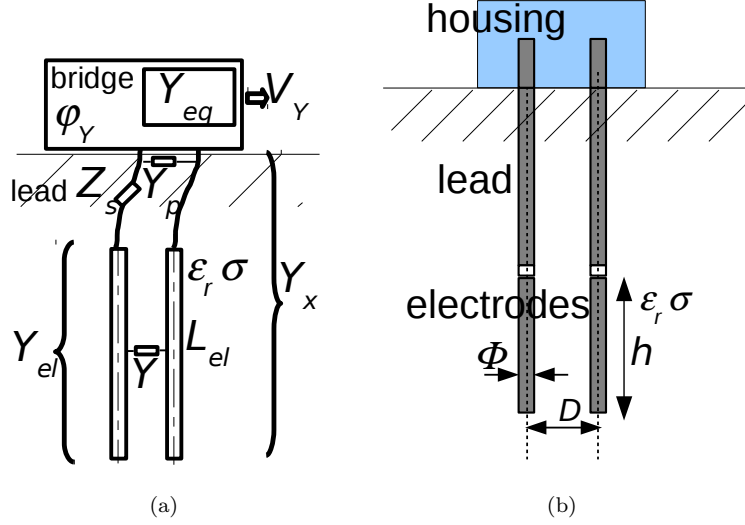


Figure 4. Sensor modeling (a) from bridge to electrodes as an electric circuit (b) geometry of lead and electrode pairs.

complex permittivity ϵ_r , by electrode inductance L_{el} and its resistance R_{el} .

Compensation of lead impedance Because the lead from bridge to electrodes - two thin wires - is always surrounded by sheath and air with constant properties, its contribution to Y_x is modeled by localized components equivalent to an impedance in series, Z_S , and an admittance in parallel, Y_p , to Y_{el} (Fig. 4(a)). Relations between Y_x and Y_{el} are thus:

$$Y_x = \frac{Y_{el} + Y_p}{1 + Z_S(Y_{el} + Y_p)} \quad \text{or} \quad Y_{el} = -Y_p + \frac{Y_x}{1 - Z_S(Y_x)}. \quad (7)$$

The admittance $Y_p = G_p + \mathbf{j}C_p 2\pi f$ is dominated by capacitive influence between wires and traces with values C_p usually lower than 1 pF.

The impedance Z_S results mainly from wire self-inductances L_S and produces non linear interferences between G_{el} and C_{el} . Development of eq. 7 shows that a conductive soil introduces in the capacitive signal a term $-G_x^2 L_S$ in F, while the conductive one contains $G_x C_x 2\pi f L_S 2\pi f$ in S. The lead between each electrode and the circuit is made of a 250- μm -thin silver-plated Cu wire. Its self-inductance, in absence of magnetic material, is a purely geometrical parameter proportional to wire length, with a coefficient of roughly 1 μH per meter. It is enclosed in a 8-mm-outer-diameter tube made of nonmagnetic stainless steel, like for electrodes. Tube is not electrically grounded as it is observed that a tube grounded from electronics side produces a perturbation on bridge output much larger than the fringing effect, which probably results from an electronic interference between electrodes and leads [Chavanne, Bruère, and Frangi (2020)].

In the case of the sensor with the deepest electrodes, with the top at 50 cm from surface, length of each lead is as high as 65 cm and, as a consequence, leads present a large inductance L_S . However, the addition in series of a capacitor of capacitance C_S permits to offset large part of L_S . Hence, the overall impedance Z_S is modeled

according to:

$$Z_S = r_S + \mathbf{j} L_S 2\pi f + \frac{1}{\mathbf{j} C_S 2\pi f} = r_S + \mathbf{j} L_S 2\pi f \left(1 - \frac{1}{L_S C_S 2\pi f^2}\right) = r_S + \mathbf{j} L'_S 2\pi f, \quad (8)$$

where L'_S is the residual lead inductance. Its precise determination requires a calibration with liquids

Wire resistance remains negligible, even accounting for skin effect at 24 MHz. However, to prevent amplifier saturation or distortion in case of short cut or presence of pure capacitance between electrodes, a small resistance r_S is added (less than 5 Ω).

Correction of electrode inductance To determine Y from Y_{el} the pair of electrodes are treated as an open-ended transmission line. It leads to the resolution of a differential equation along electrode length of which parameters include L_{el} and R_{el} , as well as Y . Taking into account the boundary conditions at electrode ends, Y_{el} corresponding to the admittance at the top ends, the solution is:

$$Y_{el} = \frac{\tanh(\gamma)}{\gamma} Y, \quad (9)$$

where \tanh is hyperbolic tangent, while γ :

$$\gamma^2 = -a + \mathbf{j} b,$$

or

$$\gamma = \sqrt{-a/2 + (\sqrt{a^2 + b^2})/2} + \mathbf{j} \sqrt{a/2 + (\sqrt{a^2 + b^2})/2},$$

with

$$\begin{cases} a = L_{el} C\omega^2 - R_{el} G, \\ b = L_{el} G\omega + R_{el} C\omega. \end{cases}$$

Assuming nonmagnetic medium and currents confined at electrode surface due to skin effect, the quantity L_{el} is mathematically linked to electrode capacitance C according to $4\pi L_{el}/\mu_0 \equiv 4\pi \varepsilon_r \varepsilon_0 h^2/C$ or $L_{el} g = \mu_0 h^2$ (μ_0 being the vacuum magnetic permeability). Therefore, in the case of electrode simple bi-cylindrical geometry inductance value is known and fixed. The same applies to R_{el} , which is found almost negligible (about 0.2 Ω).

The implicit relation between Y_{el} and Y is solved by successive iterations with $Y \equiv Y_{el}$ for the first step.

2.3. Conversions to Medium Complex Permittivity

The conductance G and the capacitance C of the admittance Y of electrodes inserted in the medium under study is related to medium permittivity ε_r and conductivity σ according to eq. 2, which depends on the geometric factor g .

As the measurement technique is independent of electrode geometry, any choice for it is possible. However, the bi-cylindrical geometry, as shown in Fig. 4(b), allows a large sample volume of soil, and, as a result, deduced soil moisture by the sensor is more representative of average soil moisture close to the sensor than a small volume. Each part of the medium contributes to sensor signal according to a weight proportional to the energy density of electric field at that part Chavanne and Frangi (2019). The density is more evenly distributed between two parallel cylinders than for two electrodes along a unique cylinder with same characteristics such as for PR2 of Delta_T. In the latter case electric energy remains concentrated too close to cylinder surface where soil has been disturbed. The situation is made worse when electrode surface is protected by a low permittivity layer - tube access like for Enviroscan sensor or a veneer - acting as a low capacitance in series with the medium. Sensor becomes insensitive to medium permittivity when increasing. It explains thus the decrease of sensitivity with soil permittivity for the planar design of the probe presented in [H. R. Bogena, Huisman, Schilling, Weuthen, and Vereecken (2017)]. In the case of the bi-cylindrical geometry the optimum requires a high electrode diameter Φ such as the ratio to electrode spacing D , Φ/D , is ideally between 0.3 to 0.5. Too thin electrodes like for Campbell's TDRs and reflectometers, including SoilVue ($\Phi/D = 0.1$), concentrate the electric field at electrode surface.

The geometry also provides a simple analytical relation for g . In the case of two parallel cylinders of height h , spacing D and diameter Φ the theoretical relation is (see appendix 2 in [Chavanne and Frangi (2019)]):

$$g_{th} = \frac{\pi h}{\operatorname{arccosh}(D/\Phi)} , \quad (10)$$

where $\operatorname{arccosh}$ is the inverse of the hyperbolic cosinus.

The value of g_{th} varies from 0.085 m (multi-channel sensors with $h = 50$ mm, $D = 100$ mm, $\Phi = 30$ mm) to 0.14 m (one-channel sensor in Fig. 1 with $h = 70$ mm, $D = 20$ mm, $\Phi = 8$ mm). The relation is valid in absence of fringing effect, i.e. with the electrode electric field in the medium independent of h , perpendicular to electrode axis and bound by the transverse planes at each electrode end. By using its whole length multi-channel sensors are designed to limit this effect to its end channels, or guards [Chavanne and Frangi (2014)]. On the other hand, the one-channel sensor with its sole pair of cylindrical electrodes is affected. It is accounted for in eq. 10 by a dimensionless factor, g/g_{th} [Chavanne et al. (2020)]. It depends mostly on the geometric ratio h/D , and tends towards 1 as the ratio increases. As sensor ratio in our case is $h/D = 3.5$, effect including both ends amounts to $g/g_{th} = 1.2$. It also raises the actual height of the sample volume, all the more as the ratio h/D is lower. However, the total increase represents less than 30% of h for the one-channel sensor (Fig. 9 in [Chavanne et al. (2020)]).

Sensor Duplication With Same Geometry Impedances in series and in parallel of lead, inductance of electrodes and **Factor** g are only geometry dependent. Tolerance on compensation capacitors is less than 1%. For sensors equipped with same wires, tubes and electrodes of identical lengths (within 1 mm of tolerance), all these parameters remain unchanged. Change of length is negligible, even taking into account thermal dilations of stainless steel and copper rods or wires (for a length l they are lower than $1/l \delta l/\delta T \sim 20 \text{ ppm}\cdot\text{C}^{-1}$).

In subsection 2.1 we have seen how to reduce close to zero bridge off-

sets and phase errors, owing in part to an on-board reference admittance. Bridges with identical components can present same sensitivities with an uncertainty of about 1%. They can be considered identical.

Consequently, for a manufacturing series of same sensors the calibration with references to determine all sensor parameters, from bridge sensitivity to g , for one or few of them would be valid for others. This point is important to build a large network of sensors without extensive costs.

2.4. *Conversions to Medium Water Content and Water Salinity*

Among the large number of available relations we have so far limited our choice to the simple Topp's correlation, obtained with TDRs [Topp et al. (1980)]. For a sandy soil made of more than 80% of quartz (less than 10% of clay), such as in the case of the Paris trial plot, the **correlation** appears appropriate. It may be less the case for a clayed calcareous soil.

As far as water pore conductivity σ_{ion} is concerned, we use the simple semi-empirical relation suggested by Hilhorst M. after validation with samples of various soils [Hilhorst (1998, 2000)]:

$$\sigma_{ion} = \frac{\sigma \varepsilon_{r_w}}{\varepsilon_r - \varepsilon_{r(\sigma=0)}} , \quad (11)$$

where ε_{r_w} is the relative permittivity of water at soil temperature.

The function assumes that the only contribution to soil conductivity σ results from ionic current in pore water. Dissipation from dipole relaxations is thus neglected. The ratio $(\varepsilon_r - \varepsilon_{r(\sigma=0)})/\varepsilon_{r_w}$ accounts for the water volume fraction to deduce σ_{ion} from σ . Hilhorst M. verified the relation from ε_r measurements on samples at different conductivities σ with a sensor operating at 20 MHz. He determined the constant $\varepsilon_{r(\sigma=0)}$, which represents the asymptotic value of medium permittivity at low σ . In absence of medium calibration, Hilhorst M. proposes the value $\varepsilon_{r(\sigma=0)} = 4.1$. However, during a dry spell in which ε_r has become low, field measurements in the case of the sandy soil have shown the necessity for a smaller value, 2 or even 1, in order to avoid extreme or negative values of σ_{ion} .

More complex relations are also available [Friedman (2005)]. Whatever the method, the quantity σ_{ion} is controlled by the difference between σ and ε_r . As a consequence, it is very sensitive to any instrument bias or phase error between permittivity and conductivity. Hilhorst suggests to restrict the use of equation 11 to sensors measuring σ and ε_r simultaneously with the same instrument, that is measuring directly the complex permittivity like in our case.

3. Results, Discussion and Perspective

3.1. *Calibration with liquids*

A calibration with various fluids of known permittivity ε_r is necessary to fix precisely some sensor parameters, especially the residual lead inductance L'_S in eq. 8. **Bridge output is converted into the admittance at bridge input thanks to eq. 5. Parasitic admittances of the lead are taken into account with eq. 7, using the expression in eq. 8. The conversion also includes the contribution of**

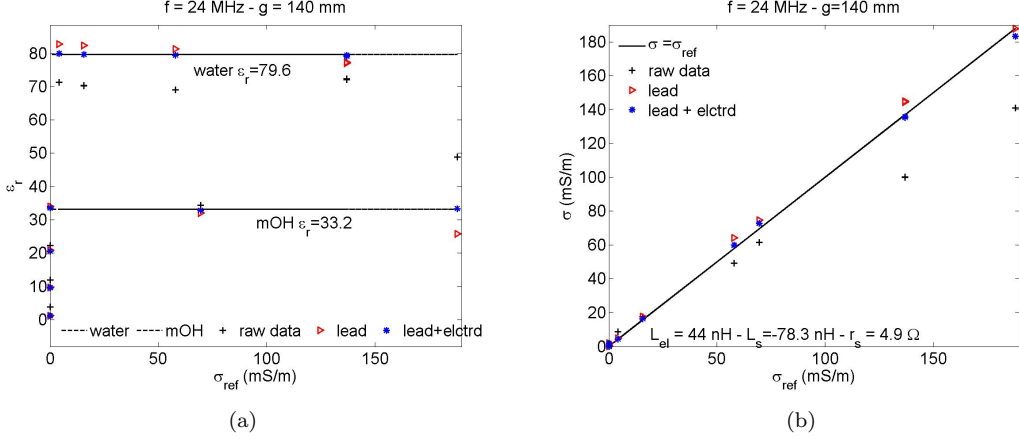


Figure 5. Calibration of a one-channel sensor fitted with a 650-mm-long lead using fluids of known permittivity ϵ_r and conductivity σ (air, octanol-1, propanol-1, methanol and water at around $T = 22^\circ\text{C}$. Methanol and water at different salinity) to adjust some parameters of the electric circuit model depicted in Figure 4(a). The main one is the residual lead inductance L'_s . Electrode geometry and dimensions impose the value of electrode inductance L_{el} . A series resistor of $r_s = 4.9 \Omega$ inserted for protection is accounted for. Plots show the influence of both inductances in the raw data. Calibration results for (a) permittivity ϵ_r (b) conductivity σ .

electrode inductance L_{el} thanks to eq. 9. Value of L_{el} is known and fixed. It is also the case for bridge sensitivity and phases, if the bridge has been adjusted and the lead is short (lower than 20 cm). Electrode admittance is converted into fluid permittivity and conductivity owing to eq. 2 and factor g given in subsection 2.3.

Fig. 5 shows the result in the case of a one-channel sensor using air, octanol-1, propanol-1, methanol and water at around $T = 22^\circ\text{C}$. For liquids only the electrodes are covered to eliminate fringing effects, as observed in a previous work [Chavanne et al. (2020)], and thus to use the factor g_{th} for conversion. Permittivity of pure alcohols are well documented, in particular from laboratory of standards [Bottreau, Dutuit, and Moreau (1977); Weast (1986-87); Gregory and Clarke (2012); Kaatze (2007)]. Variations with temperature and with frequency (due to relaxation of molecular dipoles) are given. Uncertainty from the literature is about $\delta\epsilon_r = 0.15$. Data are more accurate than values deduced from measurements performed in a non specialized laboratory (as can be inferred from overestimate by nearly 10% of the static permittivity of glycerol and propanol-1 in [Jones et al. (2005)]). Moreover, working with mixtures of liquids to reach desired permittivity adds uncertainty on reproducibility. Our setup adds some uncertainty estimated at $\delta\epsilon_r = 0.15$. Solutions of methanol at different KCl salinity, and of water, are used. Because of strong molecular dipoles the two liquids present large dissolution, which is not the case of other alcohols. Solution conductivity has been measured with conductimeter 340i of the society WTW (Germany), calibrated against standard aqueous KCl solutions. The absolute uncertainty is about $\pm 2 \mu\text{S}\cdot\text{cm}^{-1}$ with a relative uncertainty of $\pm 1\%$.

In Fig. 5 ϵ_r and σ deduced from the conversion are plotted against measured solution conductivity. The graphs show as well the result when not accounting for L'_s and/or L_{el} . As expected from equations variable ϵ_r is most affected at high salinity. Contribution of L'_s is the most important, but this depends on the compensation efficiency.

Fig. 5 corresponds to the calibration of the sensor presenting the longest lead among current prototypes, 650 mm from electrode to measuring circuit. It allows

to reach a depth of about 50 cm in soil. As a consequence, effects from propagation of electromagnetic waves along the lead wires and reflection can not be completely neglected (prototypes with short lead present a much lower effect). It represents, however, perturbations only dependent on lead characteristics. The different relations **and the number of parameters** remain unchanged, except that some parameters, bridge sensitivities and phases, differ from values at bridge level (by about +40% for sensitivities and 0.020 rad for phase errors). In total in Fig. 5 five parameters are accurately determined thanks to 9 points of calibration with liquids, each giving a permittivity and a conductivity for each sensor output, or a total of 18 values over a large range in permittivity and conductivity. Overall uncertainty for each variable is assessed at 2%, obtained for the highest conductivity. Air is used to fix precisely the complex admittance in parallel Y_p , within $\delta\varepsilon_r = \pm 0.1$ and $\delta\sigma = \pm 5 \mu\text{S}\cdot\text{cm}^{-1}$.

It is possible to extend the length beyond 65 cm to reach larger depth. Lead inductance must be tightly offset and calibration performed with care. We must assure both electrodes remain parallel mechanically.

3.2. Long Term Continuous Measurements

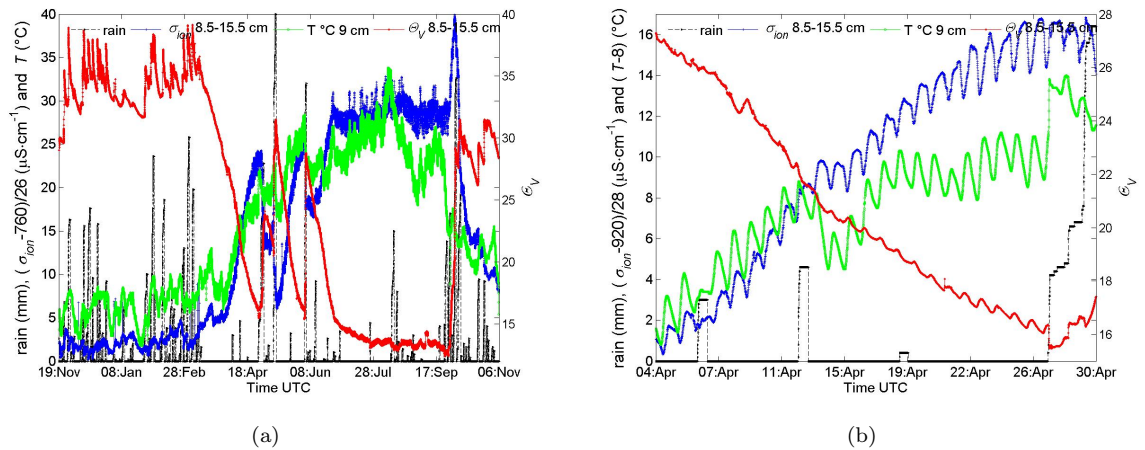


Figure 6. Monitoring of soil water content Θ_V (right hand scale), its salinity σ_{ion} (translated and reduced in left hand scale) and soil temperature T_{soil} (lhs) by a one-channel autonomous sensor in a plot on a roof in Paris (a) over the trial time; (b) over a period around 15th of April 2020. Transition from a wet and cold weather to a drier and hotter one. Precipitations from a close rain gauge are also reported (lhs).

Fig. 6(a) presents almost one year of continuous measurement of soil variables by a one-channel sensor in Paris. Data have been obtained from sensor output according to procedures and conversion relations detailed in section 2. A series from a rain gauge is also reported. The trial has taken place in a plot on the green roof of laboratory building. Over a year we observe approximately two weather patterns, a wet and cold or cool one during winter and late autumn, while summer and spring experimented drier and hotter one. Paris is submitted to various influences from a continental climate (more present in summer) to an oceanic one from Atlantic (more pronounced during winter, especially winter 2019/20 which, as a result, was one of the mildest over the last 20 years).

The same sensor has then been installed in an observatory at 800-1000 m elevation

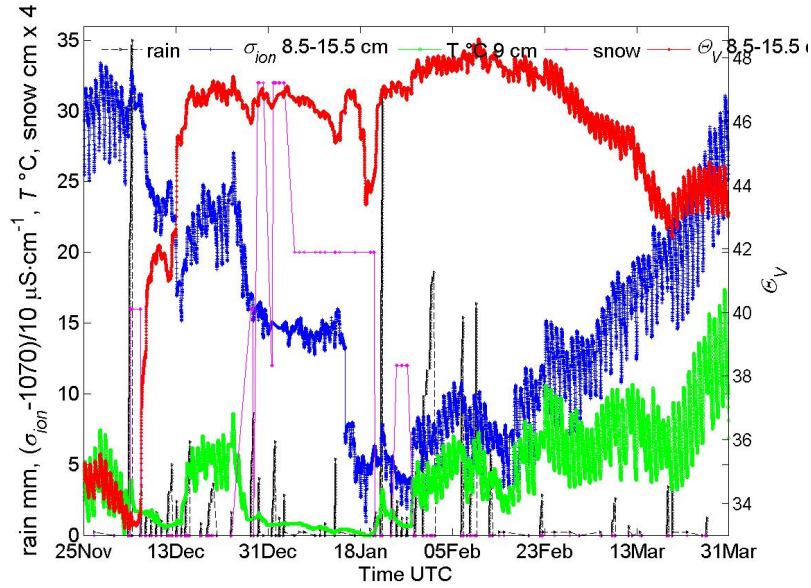


Figure 7. Series as in Fig. 6 from the same sensor since November 2020 in the observatory in Southern Alps. Winter period with occurrences of snow cover.

on sedimentary mountains, located in Southern Alps close to Digne-les-Bains. Fig. 7 shows series of the same soil variables as in Fig. 6 since sensor installation. Environment is very different from previously, with a clayey calcareous soil and a harsher weather. The plot experimented frosts and snow falls. At electrode depth no frost was observed as permittivity remained high and, therefore, water was still liquid (or nearly, as towards 22th of January Θ_V starts to drop abnormally), but probably frost occurred at soil surface. Frost and snow cover act as a thermal barrier, blocking the diurnal cycle, as well as limiting water flow. After a large rain and snow precipitation in early December, then first snow melting and lastly thaw, water content increased and remained high. From the end of December until the end of January the plot experimented again snow falls and melting with periods of cover, as reported schematically in Fig. 7. Water content started to diminish after the end of February and low precipitation. Fine structure of the clay-rich soil permits a good retention to maintain a good water content. As to be expected, σ_{ion} deduced from eq. 11 is controlled by soil temperature and flow of incoming fresh water, decreasing with both (be aware of scale translation and reduction for σ_{ion}).

By contrast, because of the nature of soil in the plot for Paris, a sand mostly made of quartz, water drains more rapidly than in Draix in absence of sufficient rain. Fig. 6(b) shows one of these periods around 15th of April. Salinity quite logically increases as soil becomes drier and warmer. Its diurnal oscillation with soil temperature is becoming more marked. An interesting feature is the apparition of a diurnal cycle as well in the series of water content. In the Alps plot too water content are modulated by diurnal cycles, especially at the end of November before the soil becomes wetter and in early spring 2021. Because of the thermal dependence of ionic conductivity in water via its viscosity, σ_{ion} and σ are naturally influenced by soil temperature T_{soil} . It is more difficult to understand the variation of Θ_V or ϵ_r . As mentioned in introduction, before any physical interpretation at soil level, effects from the instrument itself have to be ruled out or shown to be small.

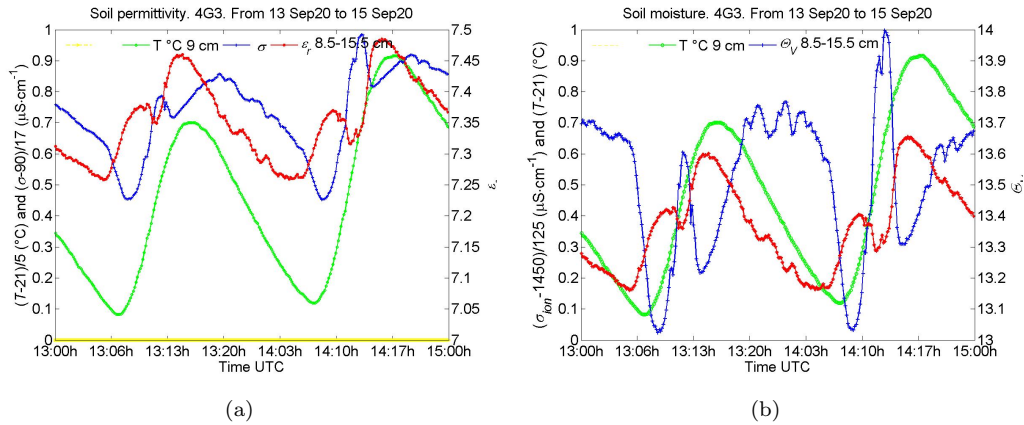


Figure 8. Soil variables against soil temperature T_{soil} corresponding to series in Fig. 6(a) over few diurnal cycles in mid-September 2020 (time in x-axis as day:hour). (a) Electric variables ε_r (right hand scale) and σ (left hand scale), and (b) physical variables water content (rhs) and its salinity (lhs).

Fig. 8(a) shows the variations of soil electrical quantities ε_r and σ , along with T_{soil} , over two diurnal cycles in September 2020 when temperatures experimented large changes. Fluctuations of ε_r and σ appear too different from each other to deduce any interference between both quantities. Moreover, it would require much larger phase error or parasitic impedance than what is left after all works to offset them, as described in section 2; conductivity presents a diurnal variation of $\delta\sigma = \pm 0.3 \text{ mS}\cdot\text{m}^{-1}$. From eq. 4 and 5 variation of $\delta\varepsilon_r = \pm 0.1$ on ε_r would require $\varphi_{G/C}$ close to 0.5 rad.

On the other hand, the series in Fig. 8(a) and 8(b) present some accidents and do not follow perfectly cycles of T_{soil} , in particular the series of σ and salinity. A potential cause is bridge electronics influenced by temperature inside the housing at soil surface. The change of weather seen in Fig. 6(b) also corresponds to a smaller sky cover, which leads to stronger variations of air temperature, and therefore of electronics temperature T_{elc} during a diurnal cycle. Sensor setup with electrodes distant from electronics makes variations of T_{soil} and T_{elc} different in time and amplitude, and permits to dissociate their effects. Its drawback is large variations of T_{elc} if no care is taken. Previously, we gave some arguments to rule out an electronic influence on the apparent oscillation of water content [Chavanne and Frangi (2014)]. However, with more available data during field trials such as that of T_{elc} and output from a reference channel in bridge circuit, we assess in more depth to which degree influence of T_{elc} is still felt, its physical origin, and hence how to further reduce it, as detailed below.

N.B.: Each sensor has a designation according to their generation and their number in it (like 4G3 or 3G1). Generation concerns the evolution of sensor system in terms of control and energy, not necessarily that of the bridge, as board of the latter is removable.

3.3. Temperature Influence Due to Electronics Drift

3.3.1. From a measuring channel

Bridge sensitivity (eq. 3) but also its phases (eq. 5) can vary with electronics drift, and hence modify the output without change at bridge input.

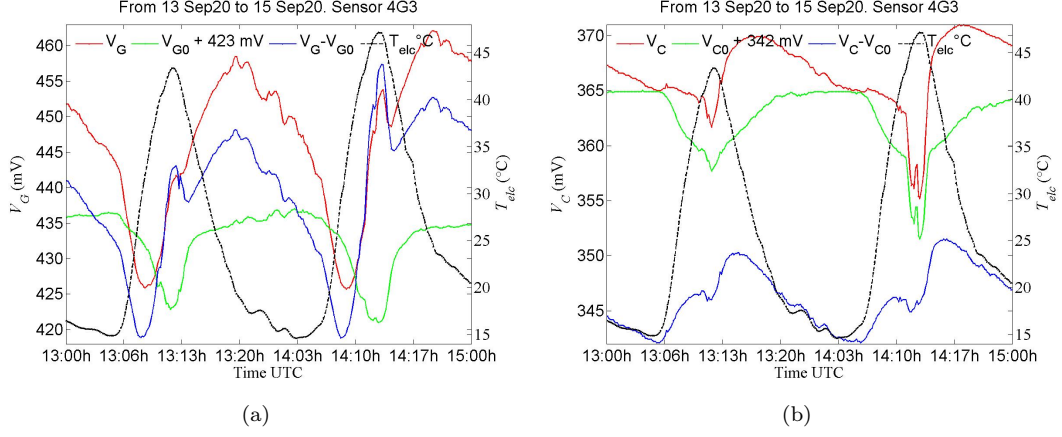


Figure 9. Bridge output corresponding to time series in Fig. 8, against electronics temperature T_{elc} (time in x-axis as day:hour). Voltages V_G and V_C are the output when bridge is connected to electrodes, while V_{G0} and V_{C0} when it is in open circuit. Voltages ΔV_G and ΔV_C are their differences. (a) Data for the G branch and (b) for the C branch.

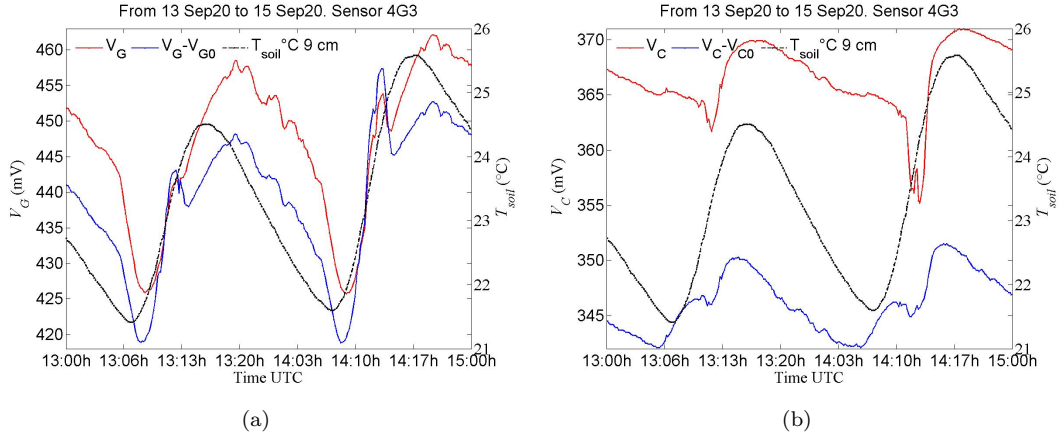


Figure 10. Same bridge outputs as in Fig. 9, except voltages V_{G0} and V_{C0} , against soil temperature T_{soil} with (a) data for the G branch and (b) for the C branch.

Fig. 9 shows variations of bridge outputs corresponding to data in Fig. 8. The time interval experimented one of the highest temperature variations over a day, both in air and soil, during the trial in Paris (Fig. 6(a)). Temperature T_{elc} is equally reported to study its influence. On day 14th of September 2020, T_{elc} rose from 15 to 45°C, or by more than $\delta T_{elc} = 30^\circ\text{C}$. As a consequence, bridge output, V_G and V_C when connected to electrodes, and V_{G0} and V_{C0} when in open circuit, present following variations, when their estimation is possible:

$$\begin{cases} \delta V_G \sim -? \text{ mV} \\ \delta V_C \sim -15 \text{ mV} \end{cases} \quad \begin{cases} \delta V_{G0} \sim -15 \text{ mV} \\ \delta V_{C0} \sim -12 \text{ mV} \end{cases} \quad \begin{cases} \delta(\Delta V_G) \sim ? \text{ mV} \\ \delta(\Delta V_C) \sim -3 \text{ mV} \end{cases}, \quad (12)$$

As they are intrinsic to bridge circuit, voltages V_{G0} and V_{C0} follow closely T_{elc} . From values in eq. 12 their dependence is about $0.5 \text{ mV}\cdot^\circ\text{C}^{-1}$, which is consistent with the temperature drift of offsets of active components reported in specifications ($\pm 0.1 \text{ mV}\cdot^\circ\text{C}^{-1}$ for one component). Its sign of variation is not relevant, as confirmed in the case of another bridge for which variations are reversed (see Fig. 11).

Output V_G and V_C is also influenced by T_{elc} variations. However, another diurnal cycle is superposed with attenuated amplitudes and shifted times. It corresponds to the influence of T_{soil} as evidenced by series in Fig. 10, in which T_{soil} is reported. Time shift between cycles is less than few hours as electrodes remain close to soil surface at about 10 cm. The difference of output, ΔV_G and ΔV_C , should cancel the influence from T_{elc} . It is not exactly the case, in particular for G branch. Changes of components in this circuit have probably created some fragility. It is not visible in a more recent bridge (see below). Both voltages still follow more closely T_{soil} than in the case of V_G and V_C . Nevertheless, determination of salinity from eq. 11 is sensitive to small perturbations on conductivity calculated from ΔV_G and, as a consequence, σ_{ion} is impacted by T_{elc} cycles as seen in Fig. 8(b).

3.3.2. From a reference channel in bridge circuit

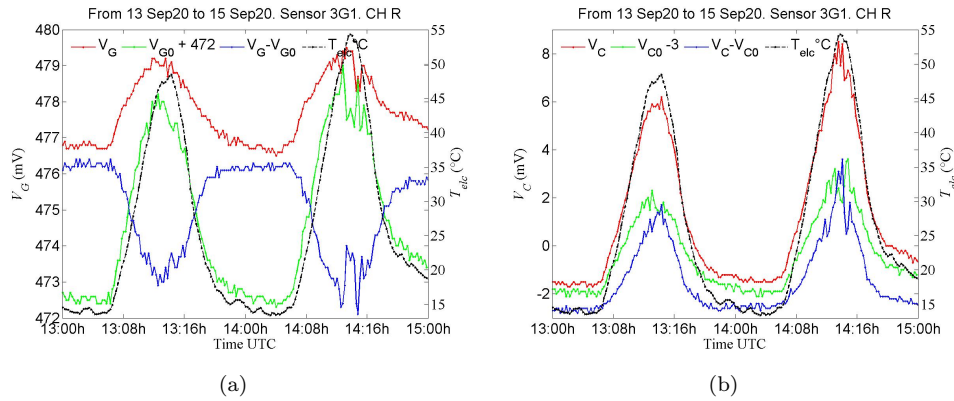


Figure 11. Bridge output for an on-board reference channel in a multi-channel sensor against electronics temperature T_{elc} during two days in mid-September 2020. (a) data for the G branch and (b) for the C branch.

The same data from a more recent bridge are also examined with the use of its reference channel constituted of a resistor of value $R_{ref} = 220 \Omega$. Output for an admittance mounted on surface board is only influenced by T_{elc} , as observed in Fig. 11, which permits a more thorough study of instrument interferences. On 14th of September, from dawn to mid-day T_{elc} rose from 15 to 55°C, or by more than $\delta T_{elc} = 40^\circ\text{C}$ (more than in the case of the one-channel sensor probably due to the type of housing for this sensor not as optimized as for the previous one). Bridge output varies accordingly:

$$\begin{cases} \delta V_{G_{ref}} \sim +3.5 \text{ mV} \\ \delta V_{C_{ref}} \sim +9.5 \text{ mV} \end{cases} \begin{cases} \delta V_{G_0} \sim +6.5 \text{ mV} \\ \delta V_{C_0} \sim +4.5 \text{ mV} \end{cases} \begin{cases} \delta(\Delta V_{G_{ref}}) \sim -3 \text{ mV}, \\ \delta(\Delta V_{C_{ref}}) \sim +5 \text{ mV}. \end{cases} \quad (13)$$

The correction of V_{G_0} and V_{C_0} is either insufficient, as in the case of $\Delta V_{C_{ref}}$, or too large, as in the case of $\Delta V_{G_{ref}}$. Output V_{G_0} and V_{C_0} permits to cancel drifts from bridge offsets but not from its gains, in particular from bridge sensitivity G_{eq} and C_{eq} (in eq. 3) and from phase shifters of functions $T_{\varphi_{C/G}}$ and $T_{\varphi_{G/C}}$ (eq. 6). The drifts from the latter ones reintroduce phase errors, $\delta\varphi_Y$, in the relations of conversion. Retaining only first order perturbations in eq. 5, relations between variations due to drifts for

the reference channel are:

$$\begin{cases} \delta^2 G_{ref} \sim \delta^2 G_{eq} (\Delta V_{G_{ref}})^2 + G_{eq}^2 \delta^2 \Delta V_{G_{ref}}, \\ \delta^2 C_{ref} (2\pi f)^2 \sim (C_{eq} 2\pi f)^2 \delta^2 \Delta V_{C_{ref}} + \delta^2 \varphi_{G/C} (G_{eq} \Delta V_{G_{ref}})^2. \end{cases} \quad (14)$$

The output $\Delta V_{C_{ref}}$ in absence of capacitance C_{ref} to measure, is still affected by T_{elc} through V_G and the drift of the shifter in the G branch.

The bridge sensitivity G_{eq} is deduced from calibration by the reference channel with data from Fig. 11(a), $G_{eq} \simeq 1/(R_{ref} \Delta V_{G_{ref}}) = 1/(0.22 \cdot 0.476) = 9.5 \text{ mS} \cdot \text{V}^{-1}$ at 20°C . For the C branch sensitivity is $C_{eq} 2\pi f \simeq 47/0.86 \cdot 0.15 = 8.1 \text{ mS} \cdot \text{V}^{-1}$ at 20°C .

Part of the drifts in bridge operations results from the temperature drift of passive components used for these operations. If surface-mount (SM) ceramic multilayer capacitors are of type COG(NPO) with a drift lower than $\pm 30 \text{ ppm} \cdot ^\circ\text{C}^{-1}$, no special care was taken in the choice of resistors. Specifications of the SM thick-film resistors in the circuit indicate a drift up to $\delta R/R \sim \pm 200 \text{ ppm} \cdot ^\circ\text{C}^{-1}$, which amounts to $\pm 0.8\%$ for $\delta T_{elc} \sim 40^\circ\text{C}$.

In the following we assume that the drifts of resistances account for observed variation of $\Delta V_{G_{ref}}$ and $\Delta V_{C_{ref}}$ in Fig. 11 via G_{eq} , the resistance in the reference channel, R_{ref} , and $\varphi_{G/C}$. Sensitivity drift $\delta^2 G_{eq}$ is assumed mainly controlled by the drift of a resistance $(\delta R/R)_{eq}$ according to:

$$\delta^2 G_{eq} \sim (\delta R/R)_{eq}^2 G_{eq}^2. \quad (15)$$

Drifts from reference components, which impair the analysis but not instrument performance, are:

$$\begin{cases} \delta^2 G_{ref} \sim \delta^2 R_{ref}/R_{ref}^4 \simeq (\delta R/R)_{ref}^2 1/R_{ref}^2, \\ \delta^2 C_{ref} (2\pi f)^2 \sim 0. \end{cases} \quad (16)$$

Drift $\delta\varphi_{G/C}$ for phase shifter of branch G is inferred from eq. 6:

$$\begin{aligned} \delta^2 \varphi_{G/C} &\simeq \delta^2 \tan \varphi_{G/C} \sim \delta^2 \left[\frac{2}{R_{\varphi_{G/C}} C_{\varphi_{G/C}} 2\pi f} \right] \\ &\sim \left[\frac{2}{R_{\varphi_{G/C}} C_{\varphi_{G/C}} 2\pi f} \right]^2 (\delta R/R)_{\varphi_{G/C}}^2. \end{aligned}$$

Hence, by combining drift assessments and values for G_{eq} and C_{eq} with the uncertainty relations in eq.14, we have:

$$\begin{cases} (\delta R/R)_{ref}^2 + (\delta R/R)_{eq}^2 \sim (\delta \Delta V_{G_{ref}} / \Delta V_{G_{ref}})^2 = (3/476)^2 \text{ or } (0.6\%)^2, \\ \delta \varphi_{G/C} \sim (\delta R/R)_{\varphi_{G/C}} / (R_{\varphi_{G/C}} C_{\varphi_{G/C}} \pi f) \sim (C_{eq} 2\pi f / G_{eq}) \delta \Delta V_{C_{ref}} / \Delta V_{G_{ref}} \simeq 1\%. \end{cases} \quad (17)$$

In the first relation, variation of ΔV_G during the diurnal cycle is consistent with the temperature drift of resistors. Moreover, when subsisting for the standard resistors in G_{eq} and R_{ref} resistors with drift lower than $\delta R/R \sim \pm 25 \text{ ppm} \cdot ^\circ\text{C}^{-1}$, drift of G_{eq} has been reduced below $\pm 100 \text{ ppm} \cdot ^\circ\text{C}^{-1}$.

Probably, drifts from other components such as the multipliers through their gain (ideally one) has to be included. Moreover, because the sign of resistor drift is

random, all gains fixed by a ratio of resistances present as well a thermal drift. All of this should explain that in the second relation of eq. 17 about bridge phase errors, the equivalent drift for $(\delta R/R)_{\varphi_{G/C}}$ is from three to five times as high as for a standard resistor. Nevertheless, substitution with a better resistor for $R_{\varphi_{G/C}}$ in the shifter has also lowered the drift on $\varphi_{G/C}$ below $\pm 150 \text{ ppm}\cdot\text{C}^{-1} \text{ rad}$, or 0.006 rad during a change of electronics temperature of 40°C .

In general, what would be the influence of a thermal phase drift on the monitoring of ε_r in presence of high soil conductivity? By differentiation of eq. 4 and approximating drift on phase θ with that on $\varphi_{G/C}$, $\delta\varphi_{G/C}$, induced error on ε_r , $\delta_{elc}\varepsilon_r$, is:

$$\delta_{elc}\varepsilon_r \sim \delta\varphi_{G/C} \frac{\sigma(\text{mS}\cdot\text{m}^{-1})}{1.33}. \quad (18)$$

For $\sigma = 200 \text{ mS}\cdot\text{m}^{-1}$, phase drift would produce an amplitude variation of $\delta_{elc}\varepsilon_r \lesssim \pm 1$ with $\delta\varphi_{G/C} \sim \pm 150 \text{ ppm}\cdot\text{C}^{-1} \text{ rad}$ and $\delta T_{elc} \simeq 40^\circ\text{C}$. Fluctuation would be in phase with that of T_{elc} , not that of soil temperature T_{soil} .

Let's examine the consequence of this relation in the case of the plot of Southern French Alps where soil conductivity is higher than in Paris plot.

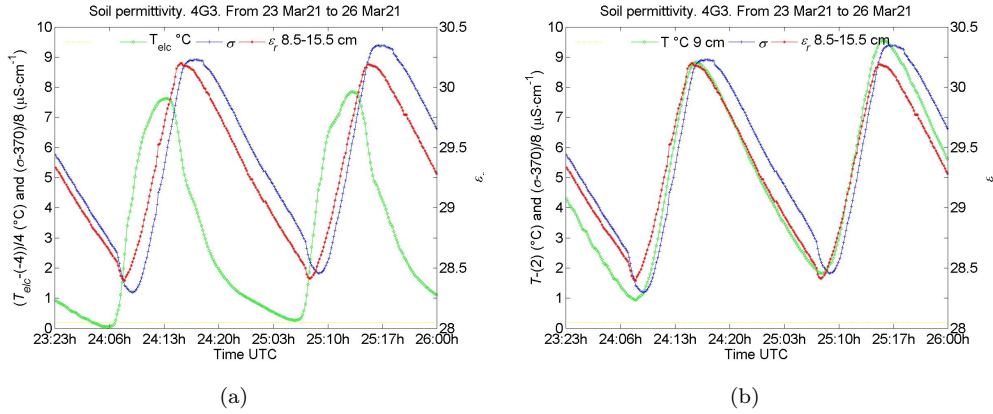


Figure 12. Soil electric variables ε_r (right hand scale) and σ (translated and reduced in lhs) corresponding to data in Fig. 7 over few diurnal cycles in early spring 2021 (time in x_axis as day:hour), (a) against electronics temperature T_{elc} (translated and reduced in lhs) and (b) against soil temperature T_{soil} (lhs).

Fig. 12 shows variations of ε_r and σ corresponding to data in Fig. 7 over few days in early spring 2021. They are reported against temperature T_{elc} and soil temperature T_{soil} . Soldering fragility of sensor bridge has been reduced. No algorithm correction is used. Taking a phase drift of $\delta\varphi_{G/C} \sim \pm 250 \text{ ppm}\cdot\text{C}^{-1} \text{ rad}$ for the bridge used, relation (18) gives an error $\delta_{elc}\varepsilon_r \sim \pm 0.15$, with $\delta T_{elc} \sim 30^\circ\text{C}$ (from -4 to 26°C) and a soil conductivity around $\sigma = 40 \text{ mS}\cdot\text{m}^{-1}$. Actually ε_r varies in phase with T_{soil} , with an amplitude of $\delta\varepsilon_r \sim 1.5$. It is modestly affected by variation of T_{elc} and a phase thermal drift. The observation confirms the result from eq. 18. Conductivity is not large enough to produce an instrumental effect. However, it shows the necessity of a low shift drift.

In this case $\delta\varepsilon_r$ is a genuine effect at soil level, independent of the instrument. As such study is beyond article scope it does not intend to find the origin of this dependency. We just notice that the change on ε_r is in phase with temperature one, which is opposite to water-permittivity dependence with temperature.

Tests in which the channel reference has only a capacitor give similar results for the drifts of sensitivity C_{eq} and phase $\varphi_{C/G}$ of the C branch.

Unitary price of resistors with tighter specification is still low (\$0.6 versus \$0.07 for standard ones, at 0.25 W w/o VAT for a purchase of 50 units). Their assembly in case of few prototypes adds fees as these components are not mounted by default on assembly machines. However, assembly for series of 50 and 100 boards will make this fixed cost negligible.

The use of these resistors to control bridge sensitivity and phases, in addition of a better thermal insulation, should avoid a correction of instrument thermal drift specific to each bridge. Nevertheless, through the reference channel in bridge circuit it is still possible to derive phase drifts $\delta\varphi_{G/C}$ and $\delta\varphi_{C/G}$. The high bridge resolution (few tenths of mV as seen in Fig. 11(a)) also permits these corrections and study these delicate effects.

4. Conclusion

The article has **provided a comprehensive description of** an in-situ sensor to monitor soil moisture and water salinity using soil permittivity ε_r and conductivity σ at a frequency 24 MHz as intermediate via an admittance approach. Soil complex permittivity presents a good sensitivity to soil quantities and numerous conversions exist in the literature. **Instrument originality relative to existing sensors lies on the use of a self-balanced Wheatstone bridge.** It is able to provide on one measurement a digital output proportional to the capacitance and conductance of electrodes in soil, hence its complex permittivity. The article has detailed from the instrument output to the electrodes all potential deviations from linearity and interferences between the two admittance parts: bridge offset and phase errors, as well as parasitic impedances. They have been modeled using electric circuit theory, and related to circuit components specifications. The work provides the means to compensate the largest part of them intrinsically or automatically (controlled relays, series capacitors and a reference admittance in bridge circuit), and analytical relations to correct residual effects, like electrode inductance.

The whole sensor is made of an electronic housing placed at ground surface and two parallel steel cylinders, with lead to bridge circuit inside and electrodes at the bottom, which are inserted in soil. The design permits easy installation from surface, low disturbances and a high sample volume around electrodes. It provides an analytical relation to convert admittance to soil permittivity and conductivity.

Calibration of a sensor with electrodes at 50-cm depth using air, alcohols and water fixes its sensitivity, as well as its residual phase and inductance, within an uncertainty of 2% over a range up to $\varepsilon_r = 80$ and $\sigma = 200 \text{ mS}\cdot\text{m}^{-1}$. Identical sensors can use same parameters after adjusting each phase errors in one simple operation.

Bridge thermal drifts during diurnal cycles and its consequences on soil variable measurement are investigated to identify physical origins. As a result, a judicious choice of resistor types permits to reduce thermal drift of phase within $\pm 150 \text{ ppm}\cdot\text{°C}^{-1}$ rad in order to keep sensor accuracy even with high conductivity and temperature changes.

Acknowledgements

This work is supported in part by the grant ANR11EQPX0011 of the Agence Nationale de la Recherche allocated to the program “Critex”—Challenging equipment for the temporal and spacial exploration of the Critical Zone at the catchment scale—(20 March 2013). It won the calls to submit projects for the “2012 Facilities of Excellence” competition named Equipex. The program Critex is a French national project, which groups together 21 laboratories from more than 20 universities and four research organizations. It will allow the study of surface and underground water relating to the characteristics of the natural environment and surrounding human activities. It will thus contribute to a better management of water resources in varied contexts. IGP contribution number: 4258

Disclosure statement

The authors declare no conflict of interest.

References

- Bechtold, M., Huisman, J., Weihermüller, L., & Vereecken, H. (2010). Accurate determination of the bulk electrical conductivity with the tdr100 cable tester. *Soil Science Society of America Journal*, *74*(2), 495–501.
- Blonquist, J., Jones, S. B., & Robinson, D. (2005). Standardizing characterization of electromagnetic water content sensors. *Vadose Zone Journal*, *4*(4), 1059–1069.
- Bogena, H., Huisman, J., Oberdörster, C., & Vereecken, H. (2007). Evaluation of a low-cost soil water content sensor for wireless network applications. *Journal of Hydrology*, *344*(1), 32–42.
- Bogena, H. R., Huisman, J. A., Schilling, B., Weuthen, A., & Vereecken, H. (2017). Effective calibration of low-cost soil water content sensors. *Sensors*, *17*(1), 208.
- Bottreau, A. M., Dutuit, Y., & Moreau, J. (1977). On a multiple reflection time domain method in dielectric spectroscopy: Application to the study of some normal primary alcohols. *The Journal of Chemical Physics*, *66*(8), 3331–3336.
- Campbell, J. E. (1990). Dielectric properties and influence of conductivity in soils at one to fifty megahertz. *Soil Science Society of America Journal*, *54*(2), 332–341.
- Chavanne, X., Bruère, A., & Frangi, J.-P. (2018). Comments to: A novel low-cost instrumentation system for measuring the water content and apparent electrical conductivity of soils, sensors, 15, 25546–25563. *Sensors*, *18*(6), 1730.
- Chavanne, X., Bruère, A., & Frangi, J.-P. (2020). Study of fringe effects of a two-rod capacitor embedded in a medium in order to deduce its permittivity. *European Journal of Environmental and Civil Engineering*, *0*(0), 1–14. Retrieved from <https://doi.org/10.1080/19648189.2020.1763477>
- Chavanne, X., & Frangi, J.-P. (2014). Presentation of a complex permittivity-meter with applications for sensing the moisture and salinity of a porous media. *Sensors*, *14*(9), 15815–15835.
- Chavanne, X., & Frangi, J.-P. (2017). Autonomous sensors for measuring continuously the moisture and salinity of a porous medium. *Sensors*, *17*(5), 1094.
- Chavanne, X., & Frangi, J.-P. (2019). Sample volume of a capacitance moisture sensor in function of its geometry. *European Journal of Environmental and Civil Engineering*, *0*(0), 1–19. Retrieved from <https://doi.org/10.1080/19648189.2018.1500311>

- Chelidze, T., & Gueguen, Y. (1999). Electrical spectroscopy of porous rocks: A review ii. experimental results and interpretation. *Geophysical Journal International*, *137*(1), 1–15.
- Chelidze, T., Gueguen, Y., & Ruffet, C. (1999). Electrical spectroscopy of porous rocks: A review i. theoretical models. *Geophysical Journal International*, *137*(1), 16–34.
- Cs650 and cs655 water content reflectometers manual [Computer software manual]. (2016, June). Logan, Utah USA.
- Debye, P. (1929). *Polar molecules*. Dover publications.
- Descarpentries, M. (1966). *Contribution à l'étude de la conductivité et de la polarisation complexe dans les milieux hétérogènes sable-argile-eau* (Tech. Rep.). Institut Français du Pétrole.
- Eller, H., & Denoth, A. (1996). A capacitive soil moisture sensor. *Journal of Hydrology*, *185*(1-4), 137–146.
- Friedman, S. P. (2005). Soil properties influencing apparent electrical conductivity: a review. *Computers and electronics in agriculture*, *46*(1-3), 45–70.
- Gaskin, G., & Miller, J. (1996). Measurement of soil water content using a simplified impedance measuring technique. *Journal of agricultural engineering research*, *63*(2), 153–159.
- Gregory, A., & Clarke, R. (2012, 01). *Tables of the complex permittivity of dielectric reference liquids at frequencies up to 5 ghz* (Tech. Rep.). National Physical Laboratory Report.
- Hilhorst, M. (1998). *Dielectric characterisation of soil* (Unpublished doctoral dissertation). Agricultural University of Wageningen, Wageningen, The Netherlands.
- Hilhorst, M. (2000). A pore water conductivity sensor. *Soil Science Society of America Journal*, *64*(6), 1922–1925.
- Jones, S. B., Blonquist, J., Robinson, D., Rasmussen, V. P., & Or, D. (2005). Standardizing characterization of electromagnetic water content sensors. *Vadose Zone Journal*, *4*(4), 1048–1058.
- Kaatze, U. (2007). Reference liquids for the calibration of dielectric sensors and measurement instruments. *Measurement Science and Technology*, *18*(4), 967.
- Kelleners, T., Soppe, R., Robinson, D., Schaap, M., Ayars, J., & Skaggs, T. (2004). Calibration of capacitance probe sensors using electric circuit theory. *Soil Science Society of America journal*, *68*(3), 770-778.
- Kessouri, P. (2012). *Mesure simultanée aux fréquences moyennes et cartographie de la permittivité diélectrique et de la conductivité électrique du sol* (Unpublished doctoral dissertation). Université Pierre et Marie Curie-Paris VI.
- Qu, W., Bogena, H., Huisman, J. A., & Vereecken, H. (2013). Calibration of a novel low-cost soil water content sensor based on a ring oscillator. *Vadose Zone Journal*, *12*(2), 1–10.
- Rêgo Segundo, A. K., Martins, J. H., Monteiro, P. M. d. B., de Oliveira, R. A., & Freitas, G. M. (2015). A novel low-cost instrumentation system for measuring the water content and apparent electrical conductivity of soils. *Sensors*, *15*(10), 25546–25563.
- Rêgo Segundo, A. K., Silva Pinto, E., Almeida Santos, G., & de Barros Monteiro, P. M. (2019). Capacitive impedance measurement: Dual-frequency approach. *Sensors*, *19*(11). Retrieved from <https://www.mdpi.com/1424-8220/19/11/2539>
- Revil, A. (2013). Effective conductivity and permittivity of unsaturated porous materials in the frequency range 1 mhz–1ghz. *Water Resources Research*, *49*(1), 306–327.
- Reynolds, S. (1970). The gravimetric method of soil moisture determination. *Journal of Hydrology*, *11*(3), 258–300.
- Rhoades, J., & Chanduvi, F. (1999). *Soil salinity assessment: Methods and interpretation of electrical conductivity measurements* (Vol. 57). Food & Agriculture Org.
- Rosenbaum, U., Huisman, J., Vrba, J., Vereecken, H., & Bogena, H. (2011). Correction of temperature and electrical conductivity effects on dielectric permittivity measurements with ech2o sensors. *Vadose zone journal*, *10*(2), 582–593.
- Rosenbaum, U., Huisman, J., Weuthen, A., Vereecken, H., & Bogena, H. (2010). Sensor-to-sensor variability of the ech o ec-5, te, and 5te sensors in dielectric liquids. *Vadose Zone Journal*, *9*(1), 181–186.
- Schmugge, T. J., Kustas, W. P., Ritchie, J. C., Jackson, T. J., & Rango, A. (2002). Remote

- sensing in hydrology. *Advances in water resources*, 25(8-12), 1367–1385.
- Sen, P., & Chew, W. C. (1983). The frequency dependent dielectric and conductivity response of sedimentary rocks. *Journal of Microwave Power*, 18(1), 95–105.
- Soilvuetm10 manual [Computer software manual]. (2019, Spt). Logan, Utah USA.
- Tdr100 user guide [Computer software manual]. (2015, June). Logan, Utah USA.
- Topp, G., Davis, J., & Annan, A. (1980). Electromagnetic determination of soil water content: Measurements in coaxial transmission lines. *Water Resources Research*, 16(3), 574–582.
- Weast, R. (Ed.). (1986-87). *CRC handbook of chemistry and physics* (67th ed.). Boca Raton, Florida, USA: CRC press.
- Zreda, M., Shuttleworth, W., Zeng, X., Zweck, C., Desilets, D., Franz, T., & Rosolem, R. (2012). Cosmos: The cosmic-ray soil moisture observing system. *Hydrology and Earth System Sciences*, 16(11), 4079–4099.